INORGANIC CHEMISTRY







FRONTIERS

RESEARCH ARTICLE

View Article Online
View Journal | View Issue



Cite this: *Inorg. Chem. Front.*, 2022, **9**, 5820

Interesting dimensional transition through changing cations as the trigger in multinary thioarsenates displaying variable photocurrent response and optical anisotropy†

Chao Zhang, a Sheng-Hua Zhou, b,c,d Yu Xiao, a Hua Lin b *b,c,d and Yi Liu b *a

Due to the intriguing component variability and structure–property flexibility, lone-pair cation-based chalcogenides have garnered substantial interest in recent years. Herein, two new multinary thioarsenates, $Cs_2ZnAs_4S_8$ and $[(NH_4)Cs]CdAs_4S_8$, were successfully discovered via a surfactant–thermal reaction. Both of them possess identical stoichiometry 2-1-4-8, but they exhibit surprisingly different structural features. $Cs_2ZnAs_4S_8$ demonstrates a three-dimensional (3D) $[ZnAs_4S_8]^{2-}$ framework made from the cornersharing $[ZnS_4]$ tetrahedra and one-dimensional (1D) $[As_4S_8]^{4-}$ chains, whereas $[(NH_4)Cs]CdAs_4S_8$ exhibits a two-dimensional (2D) $[CdAs_4S_8]^{2-}$ layer constructed from the corner-sharing $[CdS_4]$ tetrahedra and tetranuclear $[As_4S_8]$ clusters. Photoelectric measurements display that $Cs_2ZnAs_4S_8$ has higher photogenerated electron–hole pair separation efficiency than $[(NH_4)Cs]CdAs_4S_8$ under visible light irradiation. Moreover, both of them show large optical anisotropy $(\Delta n > 0.17$ at 1064 and 2050 nm), while the low dimensional structure is more conducive to enhancing the optical anisotropy based on the theoretical calculations. These findings will provide inspiration for the exploration of multifunctional chalcogenides.

Received 4th August 2022, Accepted 19th September 2022 DOI: 10.1039/d2qi01694j

Introduction

rsc.li/frontiers-inorganic

Over the past few decades, inorganic chalcogenides containing $[M^{III}Q_n]$ ($M^{III}=As$, Sb, Bi) polyhedra have attracted increasing attention because of their intriguing structural and compositional diversity. These M^{III} cations with stereochemically active lone-pair electrons are favorable to form different asymmetric coordination modes, which will further influence the electronic structures and physical properties of the resultant chalcogenides. For example, $M_2As_2Q_5$ (M=Ba, Pb; Q=S, Se) exhibit excellent overall infrared nonlinear optical (IR-NLO) performance thanks to their zero-dimensional (0D) discrete arsenate anions. Pentanary thioantimonate $Rb_2Ba_3Cu_2Sb_2S_{10}$

adopts a one-dimensional (1D) chain structure and displays a wide-bandgap and an intriguing photocurrent response.9 The narrow gap semiconductor RbBi_{11/3}Te₆, which consists of a two-dimensional (2D) infinite Bi₂Te₃-like layer, exhibits a sharp superconducting transition at ~3.2 K.4 The three-dimensional (3D) frameworks A₃Mn₂Sb₃S₈ (A = K and Rb) not only display IR-NLO performances but also possess temperaturedependent paramagnetism and photocurrent responses.¹³ On the other hand, transition-metal-based chalcogenides with d10 electronic configurations (e.g., Zn²⁺, Cd²⁺, Hg²⁺) have also been extensively investigated as these cations tend to show flexible coordination geometries, and hence engender an efficient route to design functional materials.¹⁶ For instance, $Na_6Zn_3M_2Q_9$ (M = Ga, In; Q = S, Se), 2D layered chalcogenides made of unprecedented T3-supertetrahedra, exhibit desirable photoluminescence performances. T KCd3Ga5S11 adopts a diamond-like framework structure and achieves a strong second-harmonic-generation intensity $(1.7 \times AgGaS_2)$. Ternary IR-NLO BaHgSe2 shows large susceptibility and physicochemical stability activated by the trigonal planar [HgSe₃]⁴⁻ motif.¹⁹

A tremendous amount of multinary lone-pair cation-based chalcogenides have been discovered so far, however, the systematic investigation of the A/TM/As/Q system (A = alkali metals; TM = group 12 metals; Q = chalcogen) is rarely reported. To the best of our knowledge, only 3 compounds in this system are known, namely NaCdAsS₃, ²⁰ Rb₄CdAs₂S₉, ²¹ and

[&]quot;Institute for Composites Science Innovation (InCSI), School of Materials Science and Engineering, Zhejiang University, Hangzhou 310027, China.

E-mail: liuyimse@zju.edu.cn

^bState Key Laboratory of Structural Chemistry, Fujian Institute of Research on the Structure of Matter, Chinese Academy of Sciences, Fuzhou, Fujian 350002, China. E-mail: linhua@fjirsm.ac.cn

^cFujian Science & Technology Innovation Laboratory for Optoelectronic Information of China, Fuzhou, Fujian 350108, China

^dUniversity of Chinese Academy of Sciences, Beijing 100049, China

[†] Electronic supplementary information (ESI) available: Additional experimental and theory results, together with additional tables and figures. CCDC 2167064 and 2167065. For ESI and crystallographic data in CIF or other electronic format see DOI: https://doi.org/10.1039/d2qi01694j

CsHgAsS₃.²² The first two are obtained by the solid-state method, while the last one is prepared by solvothermal synthesis. Recently, a surfactant-thermal reaction has been proved to be a facile method for exploring novel chalcogenides.²³⁻³¹ In this study, our continuous explorations based on the surfactant-thermal method have led to the discovery of two new thioarsenates, Cs₂ZnAs₄S₈ and [(NH₄)Cs]CdAs₄S₈. Although these two compounds have identical stoichiometry 2-1-4-8, they are not isostructural and undergo an interesting dimensional transition from a 3D framework to a 2D layered structure. Herein, the crystal structure, physical properties, and corresponding theoretical studies are systematically investigated.

Results and discussion

Single-crystal X-ray diffraction (SXRD) test results show that Cs₂ZnAs₄S₈ and [(NH₄)Cs]CdAs₄S₈ belong to different space

Table 1 Crystallographic data and refinement details of Cs₂ZnAs₄S₈ and [(NH₄)Cs]CdAs₄S₈

Crystal system Temperature (K) Crystal color Space group $a(\mathring{A})$ $b(\mathring{A})$ $c(\mathring{A})$ $a(\circ)$ $\beta(\circ)$ $\gamma(\circ)$ $V(\mathring{A}^3)$ Z $D_c(g cm^{-3})$ $\mu(mm^{-1})$ $GOOF on F^2$ $R_1, wR_2(I > 2\sigma(I))^a$ $R_1, wR_2(\text{all data})$	887.35 Tetragonal Yellow $I4_1/a$ (no. 88) $11.0828(5)$ $11.0828(5)$ $13.2303(8)$ 90 90 $1625.06(18)$ 4 3.627 15.004 1.039 $0.0265, 0.0603$ $0.0369, 0.0645$ $1.826/-1.271$	819.51 Tetragonal Orange P4/n (no. 85) 10.3879(2) 10.3879(2) 7.7691(2) 90 90 838.35(4) 2 3.246 12.243 1.071 0.0152, 0.0300 0.0189, 0.0316 0.818/-0.552
	887.35	819.51

^a $R_1 = \sum ||F_0| - |F_c||/\sum |F_0|, wR_2 = [\sum w(F_0^2 - F_c^2)^2/\sum w(F_0^2)^2]^{1/2}.$

groups, i.e., tetragonal I4₁/a (no. 88) for Cs₂ZnAs₄S₈ with cell parameters of a = b = 11.0828(5), c = 13.2303(8) Å, and Z = 4and tetragonal P4/n (no. 85) for [(NH₄)Cs]CdAs₄S₈ with cell parameters of a = b = 10.3879(2), c = 7.7691(2) Å, and Z = 2. The detailed crystallographic information is listed in Table 1. There are 1 unique Cs atom (Wyckoff site: 8e), 1 unique As atom (Wyckoff site: 16f), 1 unique Zn atom (Wyckoff site: 4a), and 2 unique S atoms (Wyckoff sites: 16f and 16f) in its asymmetric unit (Table 2). As illustrated in Fig. 1a, the three-dimensional (3D) crystal structure of Cs2ZnAs4S8 is constructed from charge-balanced Cs⁺ cations, regular [ZnS₄] tetrahedra, (Fig. 1b) and one-dimensional (1D) anionic chains $[As_4S_8]^{4-}$ made of the corner-sharing $[As_4S_9]$ groups (Fig. 1c). The important bond distances of Cs2ZnAs4S8 are listed in Table S1.† The As atom adopts a common coordination with 3 S atoms in the bond distance range of 2.2143(5)-2.3267(5) Å to build a [AsS₃]³⁻ triangular pyramid. The Zn-S bond distance in the [ZnS₄] tetrahedron is 2.3309(5) Å. The S-As-S angles in $Cs_2ZnAs_4S_8$ range from 98.07(2)° to 103.28(2)°, while the S–Zn– S angles vary from 105.79(2)° to 117.12(2)°. These bond distances and angles in Cs2ZnAs4S8 are normal and can also be comparable to the reported Cs-based chalcogenides. 32-34

There are 7 unique crystallographic atoms in the asymmetric unit of the structure of [(NH₄)Cs]CdAs₄S₈, including 1 Cs (Wyckoff site: 2c), 1 Cd (Wyckoff site: 2a), 1 As (Wyckoff site: 8g), 2 S (Wyckoff sites: 8g and 8g), 1 N (Wyckoff site: 2b) and 1 H (Wyckoff site: 8g) (Tables 1 and 2). As given in Fig. 1d, the crystal structure of [(NH₄)Cs]CdAs₄S₈ is composed of regular [CdS₄] tetrahedra with $d_{\text{(Cd-S)}} = 2.5481(5) \text{ Å}$ and tetranuclear [As₄S₈] clusters with $d_{\text{(As-S)}} = 2.2676(5)-2.3008(5) \text{ Å}$, which interconnect with each other by sharing vertexes to form a two-dimensional (2D) [CdAs₄S₈]²⁻ layer filling the dispersed $(NH_4)^+$ and Cs^+ cations.

The interesting structural evolution between Cs₂ZnAs₄S₈ and [(NH₄)Cs]CdAs₄S₈ is illustrated in Fig. 1. Both of them possess an identical stoichiometry of 2-1-4-8 and belong to the same tetragonal system, but they are not isostructural and have some significantly different structural features: (i) pyramidal [AsS₃] units in Cs₂ZnAs₄S₈ forms a 1D infinite [As₄S₈]⁴⁻

Table 2 Atomic coordinates and equivalent isotropic displacement parameters of Cs₂ZnAs₄S₈ and [(NH₄)Cs]CdAs₄S₈

Atom	Wyckoff	x	y	z	$U_{(\mathrm{eq})}^{a}$	Occu.
Cs ₂ ZnAs ₄ S ₈						
Cs	8 <i>e</i>	0	0.25	0.45521(2)	0.02597(6)	1.0
As	16f	0.16243(2)	0.01798(2)	0.00487(2)	0.01245(5)	1.0
Zn	4a	0	0.25	0.125	0.01320(8)	1.0
S2	16f	0.17589(5)	0.21445(4)	0.03310(3)	0.01605(9)	1.0
S1	16f	0.31599(5)	0.51563(5)	0.10909(3)	0.01892(10)	1.0
[(NH ₄)Cs]Cd					,	
Ĉs	2c	0.25	0.25	0.68028(3)	0.02210(7)	1.0
Cd	2a	0.25	0.75	0	0.01361(7)	1.0
As	8 <i>g</i>	0.04860(2)	0.15875(2)	0.14479(2)	0.01204(6)	1.0
S2	8 <i>g</i>	0.16315(4)	0.02562(4)	0.31813(6)	0.01556(10)	1.0
S1	8 <i>g</i>	0.07233(4)	0.64420(4)	0.17643(6)	0.01402(9)	1.0
N	$2\overset{\circ}{b}$	0.25	0.75	0.5	$0.0082(5)^{'}$	1.0
H	8 <i>g</i>	0.2013(19)	0.724(2)	0.446(3)	0.014(6)	1.0

 $^{^{}a}$ $U_{(eq)}$ is defined as one-third of the trace of the orthogonalized U_{ij} tensor.

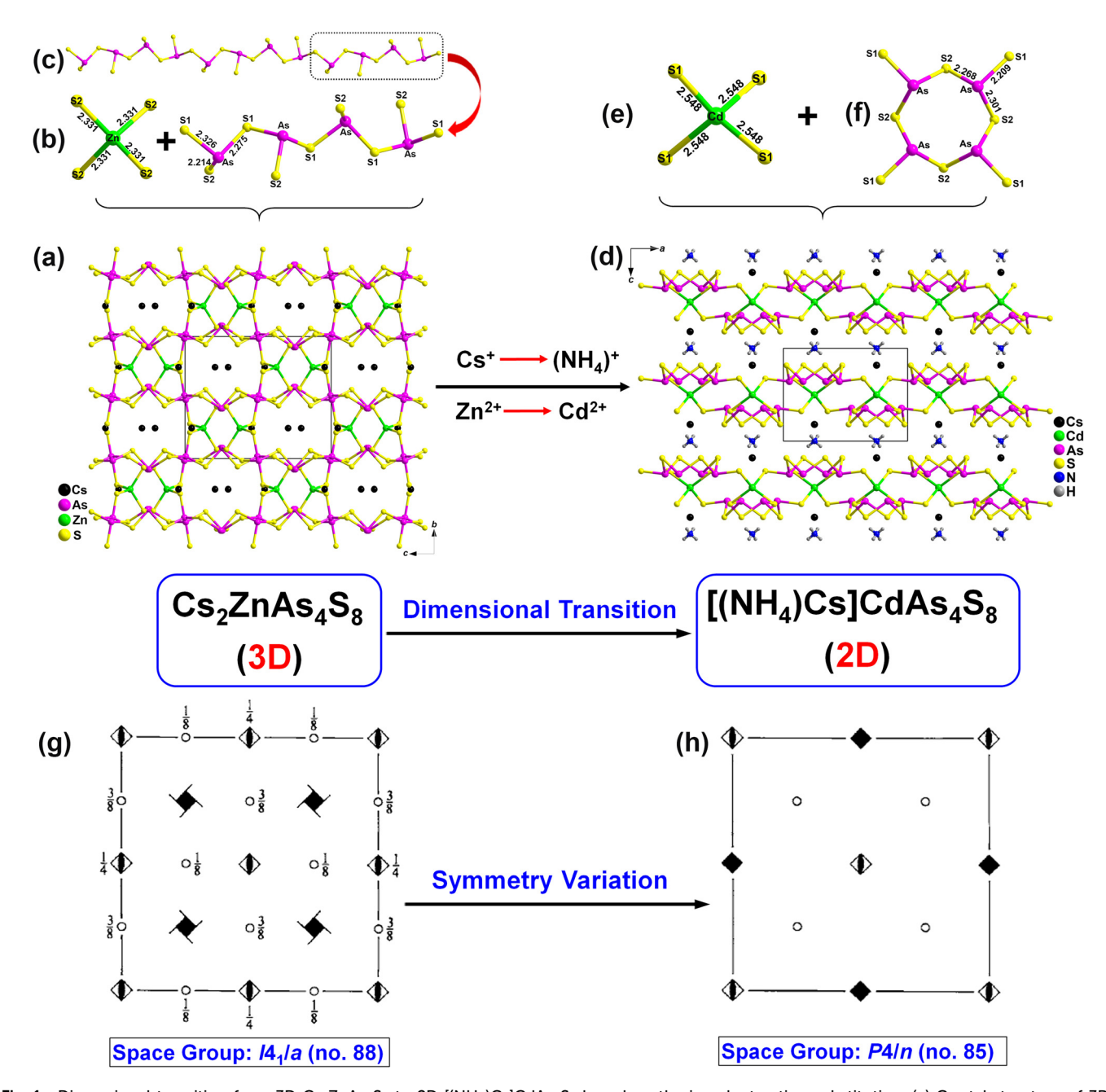


Fig. 1 Dimensional transition from 3D $Cs_2ZnAs_4S_8$ to 2D $[(NH_4)Cs]CdAs_4S_8$ based on the isovalent cation substitution. (a) Crystal structure of 3D $Cs_2ZnAs_4S_8$ viewed down the a-direction; (b) 1D $[As_4S_8]$ chain with the coordination environment of the $[As_4S_9]$ unit marked; (c) the coordination environment of the tetrahedral [ZnS₄] unit; (d) crystal structure of 2D [(NH₄)Cs]CdAs₄S₈ viewed down the a-direction; (e, f) the coordination environment of the tetrahedral [ZnS₄] unit and tetra-nuclear [As₄S₈] cluster; (g, h) spatial symmetry operation from $I4_1/a$ (no. 88) to P4/n (no. 85).

chain by vertex-sharing S1 atoms, while in [(NH₄)Cs]CdAs₄S₈, the tetra-nuclear [As₄S₈] cluster is constructed from the same [AsS₃] units; (ii) the coordination number (CN) of the crystallographically independent Cs atom in Cs2ZnAs4S8 is 10 and the Cs-S bond distances are in the range of 3.617 (5)-4.116 (6) Å, which are different from those of [(NH₄)Cs]CdAs₄S₈ [CN = 8, $d_{(Cs-S)} = 3.696(5)-3.76(5)$ Å] (Fig. S1†). Such differences between them can be attributed to the different sizes of cations, i.e., the 3D $[ZnAs_4S_8]^{2-}$ framework in $Cs_2ZnAs_4S_8$ can be viewed as [ZnS₄] tetrahedra connected by 1D infinite [As₄S₈]⁴

chains by sharing S atoms and relatively large Cs⁺ cations occupied the space of the framework. However, when one of the "large" radius Cs⁺ cations was replaced by smaller radius (NH₄)⁺ cations, the linkages between the [As₄S₈]⁴⁻ chains in Cs₂ZnAs₄S₈ are broken, and the 3D $[ZnAs_4S_8]^{2-}$ framework in $Cs_2ZnAs_4S_8$ transforms into the 0D [As₄S₈] clusters in [(NH₄)Cs]CdAs₄S₈. In addition, the above-mentioned structural evolution is ultimately reflected by their space groups, from $I4_1/a$ (for $Cs_2ZnAs_4S_8$) to P4/n(for [(NH₄)Cs]CdAs₄S₈). The detailed symmetric operation change based on isovalent cation substitution is shown in Fig. 1g and h.

Polycrystalline samples of Cs₂ZnAs₄S₈ and [(NH₄)Cs] CdAs₄S₈ were prepared by a facile surfactant-thermal method at 413 K for 7 days with CsOH·H₂O, Zn (or Cd), As₂S₃, S, oleic acid, hydrazine monohydrate (98%) and PEG-400 as staring materials, in a yield of approximately 80-90% based on Zn (or Cd) (further experimental details see the ESI†). As displayed in Fig. S2 and S3,† semi-quantitative energy-dispersive X-ray (EDX) elemental analysis provides the average atomic ratios of 2.0/1.1(2)/3.9(8)/8.2(1) and 1.0/1.1(4)/4.0(5)/7.9(7) for $Cs_2ZnAs_4S_8$ and [(NH₄)Cs]CdAs₄S₈, respectively. In addition, the purity of the polycrystalline samples was confirmed by powder X-ray diffraction (XRD) analysis (Fig. S4 and S5†). Moreover, both of them exhibit desirable thermal stability (up to 700 K) under N₂ conditions, as shown in Fig. S6 and S7.† Based on the different calculated formulas for direct semiconductors $((\alpha hv)^2)$ vs. energy) or indirect semiconductors $((\alpha h v)^{1/2} \text{ vs. energy})^{35}$ the experimental energy gaps (E_{φ}) of Cs₂ZnAs₄S₈ and $[(NH_4)Cs]$ CdAs₄S₈ are about 2.24 and 2.36 eV, respectively (Fig. 2). These values are compared to those of other reported quaternary thioarsenates, such as RbCu₄AsS₄ ($E_g = 2.15 \text{ eV}$), ³⁶ Cs₃CuAs₄S₈

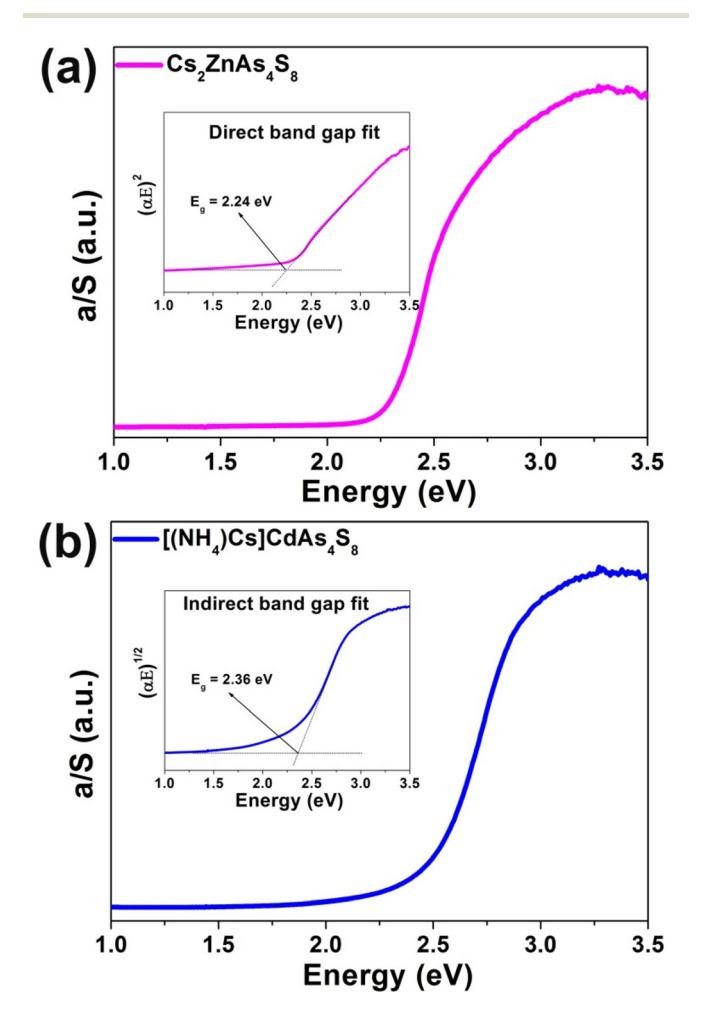


Fig. 2 UV-vis-NIR diffuse reflectance spectra of (a) $Cs_2ZnAs_4S_8$ and (b) $[(NH_4)Cs]CdAs_4S_8$ (inset: direct or indirect band gap fit based on the DFT results).

 $(E_{\rm g}$ = 2.26 eV), 30 Rb₈Cu₆As₈S₁₉ $(E_{\rm g}$ = 2.29 eV), 37 and CsCu₂AsS₃ $(E_{\rm g}$ = 2.30 eV). 27

In addition, inspired by recent reports that most of the lone-pair-based chalcogenides display intriguing photocatalytic properties, 38-43 the photoelectrochemical experiment was performed through a standard three-electrode system using simulated solar light illumination to study the photoelectric properties of Cs2ZnAs4S8 and [(NH4)Cs]CdAs4S8. As illustrated in Fig. 3, the photocurrent-time curves exhibit a rapid and consistent photocurrent response in a multiple 20 s switching period. Clearly, Cs2ZnAs4S8 shows a remarkable transient photocurrent response, which is about 4 times that of [(NH₄)Cs]CdAs₄S₈, that is, Cs₂ZnAs₄S₈ possesses higher photogenerated electron-hole pair separation efficiency than [(NH₄)Cs]CdAs₄S₈ under visible light irradiation. Meanwhile, these repeatable anodic photocurrent responses suggest that Cs₂ZnAs₄S₈ and [(NH₄)Cs]CdAs₄S₈ belong to n-type semiconductors. It is worth mentioning that these values of photocurrent densities (ca. 3.0 and 0.75 µA cm⁻² for Cs₂ZnAs₄S₈ and [(NH₄)Cs]CdAs₄S₈, respectively) are much higher than those of most recently reported chalcogenides, such as $Rb_2Ba_3Cu_2Sb_2S_{10}$ (ca. 6 nA cm⁻²), BaCuSbSe₃ (ca. 30 nA cm⁻²),³⁸ and BaCuSbS₃ (ca. 55 nA cm⁻²).³⁸

To well understand the origin of difference of electronic structures and structure–activity relationships, theoretical calculations of $Cs_2ZnAs_4S_8$ and $[(NH_4)Cs]CdAs_4S_8$ have been systematically carried out based on DFT methods. As shown in Fig. 4a and b, the valence band maximum (VBM) and the conduction band minimum (CBM) located at the same high-symmetry points (*i.e.*, Z|R) indicate that $Cs_2ZnAs_4S_8$ is a direct-band-gap ($E_g = 1.92$ eV) semiconductor, while $[(NH_4)Cs]$ $CdAs_4S_8$ is an indirect-band-gap ($E_g = 2.13$ eV) semiconductor since the VBM and the CBM are located at different high-symmetry points (*i.e.*, Z|R and V, respectively). These calculated values are slightly smaller than the experimental observations

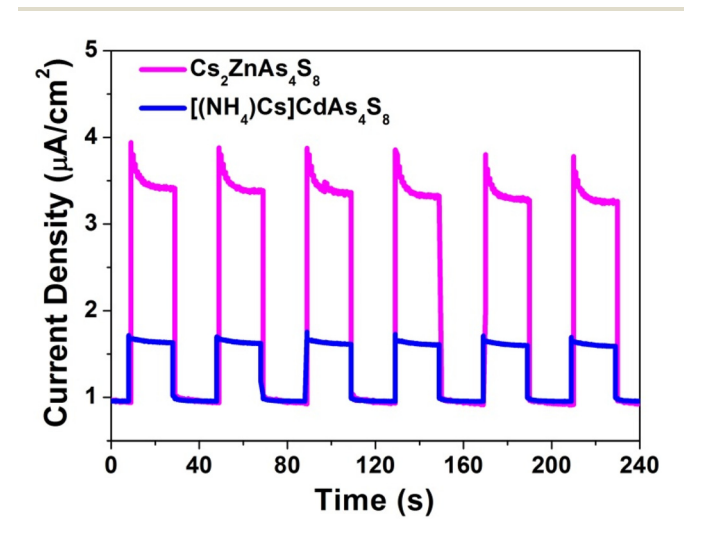


Fig. 3 Photocurrent response curves of $Cs_2ZnAs_4S_8$ and [(NH₄)Cs] $CdAs_4S_8$.

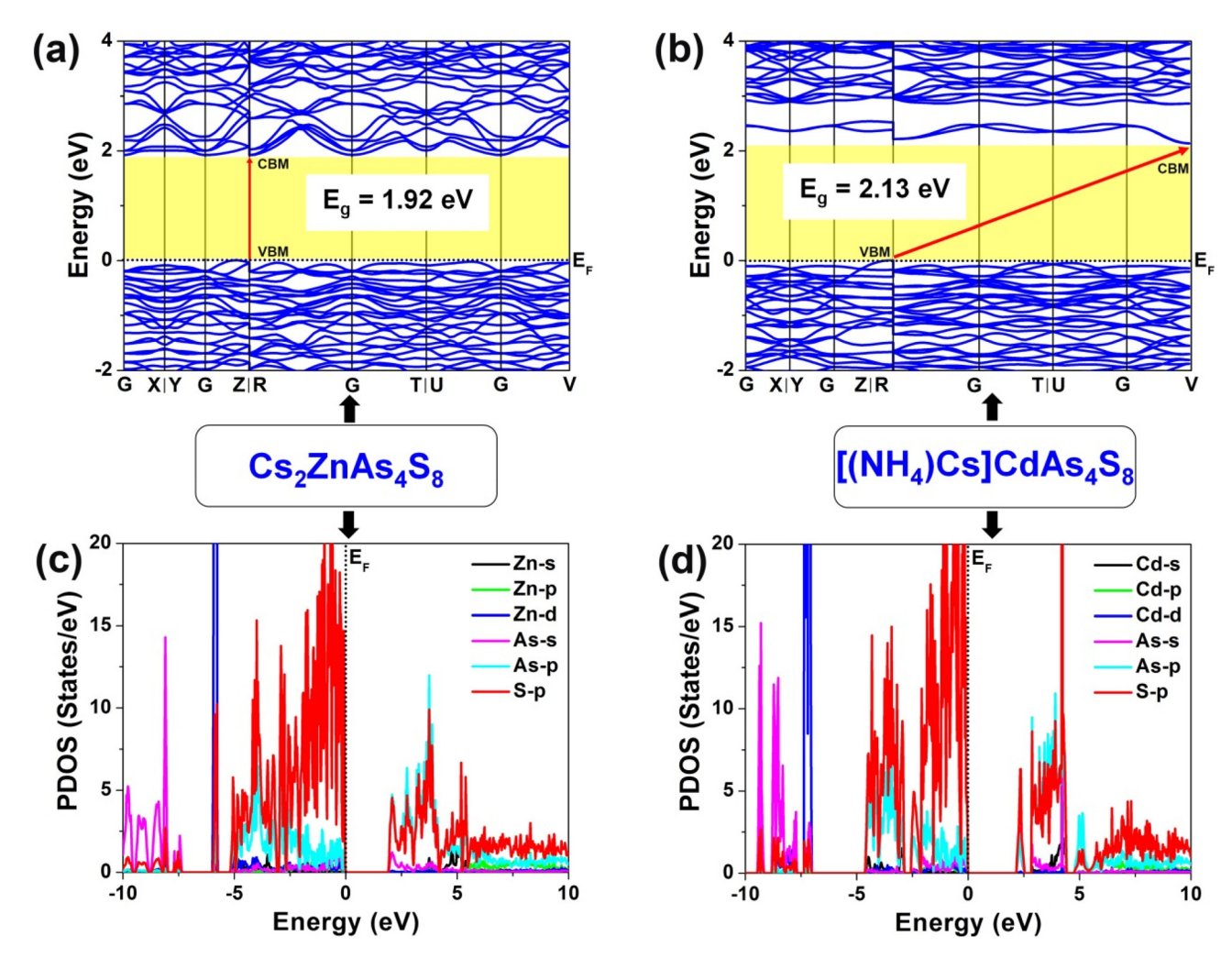


Fig. 4 Theoretical calculated results of $Cs_2ZnAs_4S_8$ and $[(NH_4)Cs]CdAs_4S_8$: (a, b) electronic band structures; (c, d) PDOSs ((states with fewer contributions are omitted for a better view). The Fermi level E_F is set at 0.0 eV.

(2.24 eV for Cs₂ZnAs₄S₈ and 2.36 eV for [(NH₄)Cs]CdAs₄S₈, as given in Fig. 2), which is a well-known phenomenon for the local approximations to DFT.44 It is widely known that the photocatalytic activity mainly depends on the separation and diffusion rate of the photogenerated charge carriers, which can be judged by calculating the relative effective masses of electrons and holes based upon the electronic structures of the VBM and CBM in the title compounds.³⁸ Through comparison, we can clearly see that the electronic bands of Cs2ZnAs4S8 are steeper than those of [(NH₄)Cs]CdAs₄S₈. Namely, Cs₂ZnAs₄S₈ is more conducive to improving the efficiency of photocatalysis, which is basically consistent with the experimental observation (Fig. 3). In addition, the projected density of states (PDOSs) with major contributions of title compounds is illustrated in Fig. 4c and d. Cs₂ZnAs₄S₈ and [(NH₄)Cs]CdAs₄S₈ exhibit similar results: the band from -5 eV to the Fermi level (EF), S-3p as well as As-4p and Zn-3d (or Cd-4d) states makes the main contribution, while the bottom of the CB is mainly composed of electronic hybridization of S-3p, As-4p and As-4s

states. Consequently, the optical Eg values of Cs2ZnAs4S8 and [(NH₄)Cs]CdAs₄S₈ mainly come from the charge transfer of Zn (or Cd)-S and As-S units, in which charge-balancing cations $(e.g., Cs^+, (NH_4)^+)$ show negligible contributions for the DOS. On the basis of their electron structures, we also calculated the birefringence (Δn) of $Cs_2ZnAs_4S_8$ and $[(NH_4)Cs]CdAs_4S_8$, respectively. As displayed in Fig. 5, their Δn values in both the important wavelengths can be calculated as 0.17@1064 nm and 0.18@2050 nm for Cs2ZnAs4S8 and 0.29@1064 nm and 0.31@2050 nm for [(NH₄)Cs]CdAs₄S₈, which are comparable with some recently reported chalcogenides, indicating that they have potential as UV-vis or IR birefringent crystals. As known, the Δn value will mainly depend on the anisotropy of the anionic substructure, whereas the contribution of chargebalancing cations can be neglected. 45-50 In other words, compared with the 3D anionic $[CdAs_4S_8]^{2-}$ framework in $[(NH_4)Cs]$ $CdAs_4S_8$, the anisotropy of the 2D anionic $[ZnAs_4S_8]^{2-}$ layer in Cs₂ZnAs₄S₈ is more obvious, which is more beneficial for producing larger Δn values.

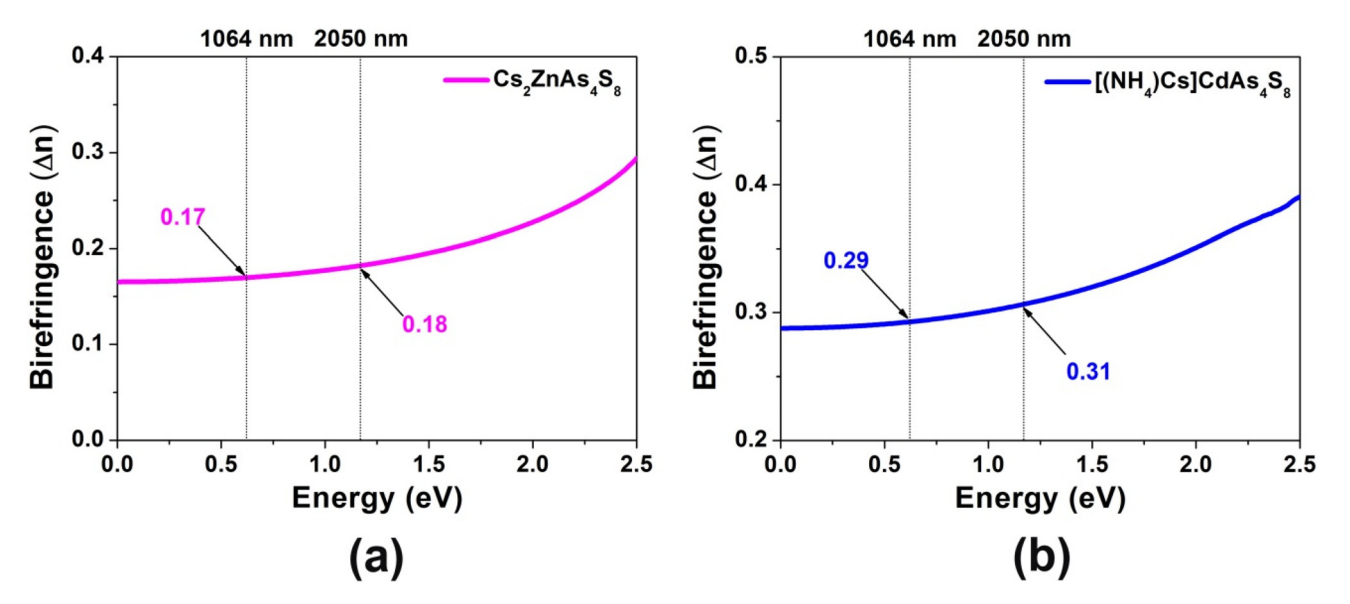


Fig. 5 Curves of the calculated birefringence (Δn) as a function of energy (eV) for (a) Cs₂ZnAs₄S₈ and (b) [(NH₄)Cs]CdAs₄S₈.

Conclusions

In conclusion, two new members of the multinary X-TM-As-S family, Cs₂ZnAs₄S₈ and [(NH₄)Cs]CdAs₄S₈, have been prepared by a simple surfactant-thermal method. Although they have similar chemical stoichiometry 2-1-4-8, they undergo an intriguing dimensional transition from a 3D framework to a 2D layered structure. The optical absorption spectra and photoelectric results confirm that both the thioarsenates are widebandgap semiconductors and Cs2ZnAs4S8 exhibits a better photocurrent response than [(NH₄)Cs]CdAs₄S₈ under the same test conditions. Meanwhile they also show large birefringence. In particular for [(NH₄)Cs]CdAs₄S₈, the calculated birefringence values are 0.29@1064 nm and 0.31@2050 nm, respectively, suggesting its potential for application as a dual-waveband birefringent crystal. The analysis results of the structure-activity relationship show that the low dimensional structure of this family will be favorable for the generation of large optical anisotropy, that is, to obtain high birefringence. These results provide new insights into the exploration of novel functional chalcogenides and further research on the other physical properties of the title compounds is ongoing.

Author contributions

C. Zhang prepared the samples, and designed and carried out the experiments. S. H. Zhou carried out the theoretical calculations. Y. Xiao measured the optical properties. H. Lin and Y. Liu conceived the experiments, analyzed the results and wrote and edited the manuscript. All the authors have approved the final version of the manuscript.

Conflicts of interest

There are no conflicts to declare.

Acknowledgements

This work was supported by the National Natural Science Foundation of China (No. 52171277, 22175175 and 21771179), the Natural Science Foundation of Fujian Province (No. 2019J01133), the Fujian Science & Technology Innovation Laboratory for Optoelectronic Information of China (2021ZR118) and the Shanxi-Zheda Institute of Advanced Materials and Chemical Engineering (2022SZ-TD006).

References

- 1 T. K. Bera, J. I. Jang, J. B. Ketterson and M. G. Kanatzidis, Strong Second Harmonic Generation from the Tantalum Thioarsenates $A_3Ta_2AsS_{11}$ (A = K and Rb), J. Am. Chem. Soc., 2009, 131, 75-77.
- D. Malliakas, D. Y. Chung, H. Claus and M. G. Kanatzidis, Superconductivity in the Narrow-Gap Semiconductor CsBi₄Te₆, J. Am. Chem. Soc., 2013, 135, 14540-14543.
- 3 L. L. Long, A. Y. Zhang, Y. X. Huang, X. Zhang and H. Q. Yu, A robust cocatalyst Pd₄S uniformly anchored onto Bi₂S₃ nanorods for enhanced visible light photocatalysis, J. Mater. Chem. A, 2015, 3, 4301-4306.
- 4 C. D. Malliakas, D. Y. Chung, H. Claus and M. G. Kanatzidis, Superconductivity in the Narrow Gap Semiconductor RbBi_{11/3}Te₆, J. Am. Chem. Soc., 2016, 138, 14694-14698.

5 G. J. Tan, L. D. Zhao and M. G. Kanatzidis, Rationally Designing **High-Performance** Bulk Thermoelectric Materials, Chem. Rev., 2016, 116, 12123-12149.

Research Article

- 6 N. Markus, F. Felix, K. Marcus and O. Oliver, Single crystal structure elucidation and thermoelectric properties of a long-periodically ordered germanium arsenic telluride, J. Alloys Compd., 2017, 694, 1160-1164.
- 7 H. Lin, Y. Y. Li, M. Y. Li, Z. J. Ma, L. M. Wu, X. T. Wu and Q. L. Zhu, Centric-to-acentric structure transformation induced by a stereochemically active lone pair: a new insight for design of IR nonlinear optical materials, I. Mater. Chem. C, 2019, 7, 4638-4643.
- 8 P. Levinsky, C. Candolfi, A. Dauscher, J. Tobola, J. Heitmánek and B. Lenoir, Thermoelectric properties of the tetrahedrite-tennantite solid solutions Cu₁₂Sb_{4-x}As_xS₁₃ and $Cu_{10}Co_2Sb_{4-y}As_yS_{13}$ (0 \leq x, y \leq 4), Phys. Chem. Chem. Phys., 2019, 21, 4547-4555.
- 9 C. Liu, Y. Xiao, H. Wang, W. X. Chai, X. F. Liu, D. M. Yan, H. Lin and Y. Liu, One-Dimensional Chains in Pentanary Chalcogenides A₂Ba₃Cu₂Sb₂S₁₀ (A = K, Rb, Cs) Displaying a Photocurrent Response, Inorg. Chem., 2020, 59, 1577-1581.
- 10 H. Lin, W. B. Wei, H. Chen, X. T. Wu and Q. L. Zhu, Rational design of infrared nonlinear optical chalcogenides by chemical substitution, Coord. Chem. Rev., 2020, 406, 213150.
- 11 M. Yan, H.-G. Xue and S.-P. Guo, Recent Achievements in Lone-Pair Cation-Based Infrared Second-Order Nonlinear Optical Materials, Cryst. Growth Des., 2021, 21, 698-720.
- 12 M.-M. Chen, Z. Ma, B.-X. Li, W.-B. Wei, X.-T. Wu, H. Lin and Q.-L. Zhu, $M_2As_2Q_5$ (M = Ba, Pb; Q = S, Se): a source of infrared nonlinear optical materials with excellent overall performance activated by multiple discrete arsenate anions, J. Mater. Chem. C, 2021, 9, 1156-1163.
- 13 Y. Xiao, M. M. Chen, Y. Y. Shen, P. F. Liu, H. Lin and Y. Liu, $A_3Mn_2Sb_3S_8$ (A = K and Rb): a new type of multifunctional infrared nonlinear optical material based on unique threedimensional open frameworks, Inorg. Chem. Front., 2021, 8, 2835-2843.
- 14 M.-M. Chen, S.-H. Zhou, W.-B. Wei, B.-X. Li, M.-Y. Ran, X.-T. Wu, H. Lin and Q.-L. Zhu, RbBiP₂S₆: A Promising IR Nonlinear Optical Material with a Giant Second-Harmonic Generation Response Designed by Aliovalent Substitution, ACS Mater. Lett., 2022, 4, 1264-1269.
- 15 H. Chen, M.-Y. Ran, W.-B. Wei, X.-T. Wu, H. Lin and Q.-L. Zhu, A comprehensive review on metal chalcogenides with three-dimensional frameworks for infrared nonlinear optical applications, Coord. Chem. Rev., 2022, 470, 214706.
- 16 H. Chen, W. B. Wei, H. Lin and X. T. Wu, Transition-metalbased chalcogenides: A rich source of infrared nonlinear optical materials, Coord. Chem. Rev., 2021, 448, 214154.
- 17 A. Abudurusuli, K. Wu, Y. Rouzhahong, Z. Yang and S. Pan, $Na_6Zn_3M_{2}^{III}Q_9$ (M_{2}^{III} = Ga, In; Q = S, Se): four new supertetrahedron-layered chalcogenides with unprecedented vertex-sharing T₃-clusters and desirable photoluminescence performances, Inorg. Chem. Front., 2018, 5, 1415-1422.

- 18 M.-M. Chen, S.-H. Zhou, W.-B. Wei, X.-T. Wu, H. Lin and Q.-L. Zhu, Phase Matchability Transformation in the Infrared Nonlinear Optical Materials with Diamond-Like Frameworks, Adv. Opt. Mater., 2022, 10, 2102123.
- 19 C. Li, W. Yin, P. Gong, X. Li, M. Zhou, A. Mar, Z. Lin, J. Yao, Y. Wu and C. Chen, Trigonal Planar [HgSe₃]⁴⁻ Unit: A New Kind of Basic Functional Group in IR Nonlinear Optical Materials with Large Susceptibility and Physicochemical Stability, J. Am. Chem. Soc., 2016, 138, 6135-6138.
- 20 Y. D. Wu and W. Bensch, Synthesis, crystal structures, and optical properties of NaCdPnS₃ (Pn = As, Sb), I. Alloys Compd., 2012, 511, 35-40.
- 21 R. G. lyer and M. G. Kanatzidis, $[Mn_2(AsS_4)_4]^{8-}$ and [Cd₂(AsS₄)₂(AsS₅)₂]⁸⁻: Discrete Clusters with High Negative Charge from Alkali Metal Polythioarsenate Fluxes, Inorg. Chem., 2004, 43, 3656-3662.
- 22 X. Y. Tian, C. X. Du, G. T. ZhaoRi, M. G. SheLe, Y. S. Bao and M. H. Baiyin, The solvothermal synthesis and characterization of quaternary arsenic chalcogenides CsTMAsQ3 (TM = Hg, Cd; Q = S, Se) using Cs^+ as a structure directing agent: from 1D anionic chains to 2D anionic layers, RSC Adv., 2020, 10, 34903-34909.
- 23 W. W. Xiong, E. U. Athresh, Y. T. Ng, J. Ding, T. Wu and Q. C. Zhang, Growing Crystalline Chalcogenidoarsenates in Surfactants: From Zero-Dimensional Cluster to Three-Dimensional Framework, J. Am. Chem. Soc., 2013, 135, 1256-1259.
- 24 W. W. Xiong, P. Z. Li, T. H. Zhou, A. Y. Tok, R. Xu, Y. Zhao and Q. C. Zhang, Kinetically Controlling Phase Transformations of Crystalline Mercury Selenidostannates through Surfactant Media, Inorg. Chem., 2013, 52, 4148-4150.
- 25 C. Liu, Y. Y. Shen, P. P. Hou, M. J. Zhi, C. M. Zhou, W. X. Chai, J. W. Cheng and Y. Liu, Hydrazine-Hydrothermal Synthesis and Characterization of the Two New Quaternary Thioantimonates(III) BaAgSbS3 and BaAgSbS₃·H₂O, *Inorg. Chem.*, 2015, **54**, 8931–8936.
- 26 W. W. Xiong and Q. C. Zhang, Surfactants as Promising Media for the Preparation of Crystalline Inorganic Materials, Angew. Chem., Int. Ed., 2015, 54, 11616-11623.
- 27 Y. Y. Shen, C. Liu, P. P. Hou, M. J. Zhi, C. M. Zhou, W. X. Chai, Q. C. Zhang and Y. Liu, Facile surfactantthermal syntheses and characterization of quaternary copper thioantimonates(III) ACu₂SbS₃ (A = K, Rb, Cs), J. Alloys Compd., 2016, 660, 171-177.
- 28 D. M. Yan, P. P. Hou, C. Liu, W. X. Chai, X. R. Zheng, L. D. Zhang, M. J. Zhi, C. M. Zhou and Y. Liu, Effect of alkali cations on two-dimensional networks of two new quaternary thioarsenates (III) prepared by a facile surfactant-thermal method, J. Solid State Chem., 2016, 241, 47-53.
- 29 D. M. Yan, C. Liu, W. X. Chai, X. R. Zheng, L. D. Zhang, M. J. Zhi, C. M. Zhou, Q. C. Zhang and Y. Liu, Facile Hydrazine-Hydrothermal Syntheses and Characterizations of Two Quaternary Thioarsenates(III): Two-Dimensional

- SrAg₄As₂S₆·2H₂O and One-Dimensional BaAgAsS₃, *Chem. Asian J.*, 2016, 11, 1842–1848.
- 30 D. M. Yan, Y. Xiao, C. Liu, P. P. Hou, W. X. Chai, H. Hosono, H. Lin and Y. Liu, Two new members in the quaternary Cs-Ag-As-S family with different arrangements of Ag-S and As-S asymmetric building units: syntheses, structures, and theoretical studies, *Dalton Trans.*, 2020, 49, 9743–9750.
- 31 R. Ye, B. W. Liu, X. M. Jiang, J. Lu, H. Y. Zeng and G. C. Guo, $AMnAs_3S_6$ (A = Cs, Rb): Phase-Matchable Infrared Nonlinear Optical Functional Motif $\left[As_3S_6\right]^{3-}$ Obtained via Surfactant–Thermal Method, *ACS Appl. Mater. Interfaces*, 2020, **12**, 53950–53956.
- 32 H. Lin, L. J. Zhou and L. Chen, Sulfides with Strong Nonlinear Optical Activity and Thermochromism: $ACd_4Ga_5S_{12}$ (A = K, Rb, Cs), *Chem. Mater.*, 2012, **24**, 3406–3414.
- 33 H. Lin, H. Chen, Y. J. Zheng, J. S. Yu, X. T. Wu and L. M. Wu, Coexistence of Strong Second Harmonic Generation Response and Wide Band Gap in AZn₄Ga₅S₁₂ (A = K, Rb, Cs) with 3D Diamond-like Frameworks, *Chem. Eur. J.*, 2017, 23, 10407–10412.
- 34 Y. J. Zheng, Y. F. Shi, C. B. Tian, H. Lin, L. M. Wu, X. T. Wu and Q. L. Zhu, An Unprecedented Pentanary Chalcohalide with the Mn Atoms in Two Chemical Environments: Unique Bonding Characteristics and Magnetic Properties, *Chem. Commun.*, 2019, 55, 79–82.
- 35 J. Tauc, R. Grigorovici and A. Vancu, Optical Properties and Electronic Structure of Amorphous Germanium, *Phys. Status Solidi*, 1966, 15, 627.
- 36 Y. Takeuchi and N. Haga, On the crystal structures of seligmannite, PbCuAsS₃, and related minerals, *Z. Kristallogr. Cryst. Mater.*, 1969, **130**, 254–260.
- 37 H. G. Yao, M. Ji, S. H. Ji and Y. L. An, Synthesis, structure and characterization of two new copper(I)-thioarsenates (III) constructed by the [AsS₃]³⁻ and CuS_x units, *J. Solid State Chem.*, 2013, **198**, 289–294.
- 38 C. Liu, P. P. Hou, W. X. Chai, J. W. Tian, X. R. Zheng, Y. Y. Shen, M. J. Zhi, C. M. Zhou and Y. Liu, Hydrazine-hydrothermal syntheses, characterizations and photoelectrochemical properties of two quaternary chalcogenidoantimonates (III) BaCuSbQ₃ (Q = S, Se), *J. Alloys Compd.*, 2016, 679, 420–425.
- 39 C. Li, Z. Lin, L. Kang, Z. Lin, H. Huang, J. Yao and Y. Wu, Sn₂SiS₄, synthesis, structure, optical and electronic properties, *Opt. Mater.*, 2015, 47, 379–385.
- 40 L. N. Nie and Q. C. Zhang, Recent progress in crystalline metal chalcogenides as efficient photocatalysts for organic

- pollutant degradation, *Inorg. Chem. Front.*, 2017, 4, 1953-1962.
- 41 L. N. Nie, G. F. Liu, J. Xie, T. T. Lim, G. S. Armatas, R. Xu and Q. C. Zhang, Syntheses, crystal structures, and photocatalytic properties of two ammonium-directed Ag-Sb-S complexes, *Inorg. Chem. Front.*, 2017, 4, 954–959.
- 42 M.-Y. Ran, S.-H. Zhou, W.-B. Wei, B.-J. Song, Y.-F. Shi, X.-T. Wu, H. Lin and Q.-L. Zhu, Quaternary Chalcohalides CdSnSX₂ (X = Cl or Br) with Neutral Layers: Syntheses, Structures, and Photocatalytic Properties, *Inorg. Chem.*, 2021, **60**, 3431–3438.
- 43 M.-Y. Li, X.-Y. Xie, X.-T. Wu, X.-F. Li and H. Lin, Quaternary Selenophosphate Cs₂ZnP₂Se₆ Featuring Unique Onedimensional Chains and Exhibiting Remarkable Photoelectrochemical Response, *Chin. J. Struct. Chem.*, 2021, 40, 246–255.
- 44 K. Burke, Perspective on density functional theory, *J. Chem. Phys.*, 2012, **136**, 150901.
- 45 M. Y. Ran, Z. J. Ma, H. Chen, B. X. Li, X. T. Wu, H. Lin and Q. L. Zhu, Partial Isovalent Anion Substitution to Access Remarkable Second-Harmonic Generation Response: A Generic and Effective Strategy for Design of Infrared Nonlinear Optical Materials, *Chem. Mater.*, 2020, 32, 5890– 5896.
- 46 M.-Y. Ran, Z. Ma, X.-T. Wu, H. Lin and Q.-L. Zhu, Ba₂Ge₂Te₅: a ternary NLO-active telluride with unusual one-dimensional helical chains and giant second-harmonic-generation tensors, *Inorg. Chem. Front.*, 2021, **8**, 4838–4845.
- 47 C. Liu, S.-H. Zhou, C. Zhang, Y.-Y. Shen, X.-Y. Liu, H. Lin and Y. Liu, CsCu₃SbS₄: rational design of a two-dimensional layered material with giant birefringence derived from Cu₃SbS₄, *Inorg. Chem. Front.*, 2022, **9**, 478–484.
- 48 M.-Y. Ran, S.-H. Zhou, B.-X. Li, W.-B. Wei, X.-T. Wu, H. Lin and Q.-L. Zhu, Enhanced Second-Harmonic-Generation Efficiency and Birefringence in Melillite Oxychalcogenides Sr₂MGe₂OS₆ (M = Mn, Zn, and Cd), *Chem. Mater.*, 2022, 34, 3853–3861.
- 49 H.-D. Yang, M.-Y. Ran, S.-H. Zhou, X.-T. Wu, H. Lin and Q.-L. Zhu, Rational Design via Dual-Site Aliovalent Substitution Leads to an Outstanding IR Nonlinear Optical Material with Well-Balanced Comprehensive Properties, Chem. Sci., 2022, 13, 10725–10733.
- 50 Y.-F. Shi, Z. Ma, B.-X. Li, X.-T. Wu, H. Lin and Q.-L. Zhu, Phase matching achieved by isomorphous substitution in IR nonlinear optical material Ba₂SnSSi₂O₇ with an undiscovered [SnO₄S] functional motif, *Mater. Chem. Front.*, 2022, DOI: 10.1039/D2QM00621A.